Electronic Supplementary Information (ESI)

Synthesis, Spectroscopic, Electrochemical Redox, Solvatochromism and Anion Binding Properties of β-Tetra- and -Octaphenylethynyl Substituted *Meso*-Tetraphenylporphyrins

Ravi Kumar, Pinky Yadav, Pinki Rathi and Muniappan Sankar*

Department of Chemistry, Indian Institute of Technology Roorkee, Roorkee - 247667, India

Table of contents

	Page No.
Figure S1. ^{1}H NMR spectrum of $H_2TPP(PE)_4$ in $CDCl_3$ at 298 K	3
Figure S2. ^{1}H NMR spectrum of $ZnTPP(PE)_4$ in $CDCl_3$ at 298 K	3
Figure S3. ^{1}H NMR spectrum of $NiTPP(PE)_4$ in $CDCl_3$ at 298 K	4
Figure S4. ^{1}H NMR spectrum of $H_2TPP(PE)_8$ in $CDCl_3$ at 298 K	4
Figure S5. ^{1}H NMR spectrum of $ZnTPP(PE)_8$ in $CDCl_3$ at 298 K	5
Figure S6. ^{1}H NMR spectrum of $NiTPP(PE)_8$ in $CDCl_3$ at 298 K	5
Figure S7. MALDI-TOF mass spectrum of $H_2TPP(PE)_4$	6
Figure S8. MALDI-TOF mass spectrum of $ZnTPP(PE)_4$	6
Figure S9. MALDI-TOF mass spectrum of $CuTPP(PE)_4$	7
Figure S10. MALDI-TOF mass spectrum of $NiTPP(PE)_4$	7
Figure S11. MALDI-TOF mass spectrum of $H_2TPP(PE)_8$	8
Figure S12. MALDI-TOF mass spectrum of $CuTPP(PE)_8$	8
Figure S13. MALDI-TOF mass spectrum of $CoTPP(PE)_8$	9
Figure S14. MALDI-TOF mass spectrum of $NiTPP(PE)_8$	9
Figure S15. MALDI-TOF mass spectrum of $ZnTPP(PE)_8$	10
Figure S16. The ORTEP diagrams showing top and side views of $H_2T(4\text{-BuPh})P(PE)_4$ (a and b); $H_2TPP(PE)_8$ (c and d) ; $ZnTPP(PE)_4$ (e and f) and $ZnTPP(PE)_8$ (g and h). The solvates are not shown for clarity, and in side view, the β-substituents and meso-phenyl groups are not shown for clarity.	11
Figure S17. The ORTEP diagrams showing top and side views of $CuT(4\text{-BuPh})P(PE)_4$ (a and b); $CuTPP(PE)_8$ (c and d) and $NiTPP(PE)_8$ (e and f). The solvates are not shown for clarity, and in side view, the β-substituents and meso-phenyl groups are not shown for clarity.	12
Table S1. Crystal structure data of β-phenylethynyl substituted porphyrins from literature.	13

Figure S18. Fluorescence spectra of $ZnTPP(PE)_n$ (n = 4 and 8) in CH_2Cl_2 at 298 K.	13
Figure S19. Cyclic Voltammograms of (a) $ZnTPP(PE)_n$ (n = 0, 4 and 8); (b) $MTPP(PE)_4$; (c) $MTPP(PE)_8$ where M = 2H, Co(II), Ni(II), Cu(II) and Zn(II); in CH_2Cl_2 containing 0.1 M $TBAPF_6$ using Ag/AgCl as reference electrode with a scan rate of 0.1 V/sat 298 K.	14
Table S2. Electrochemical redox data (vs Ag/AgCl) of $CoTPP(PE)_n$ (n = 0, 4 and 8) using 0.1 M $TBAPF_6$ with a scan rate of 0.1 V/s at 298 K.	15
Figure S20. HOMO-LUMO gap variation in $MTPP(PE)_n$ (M = 2H, Zn(II) and Ni(II); n = 0, 4 and 8).	15
Figure S21. UV-Visible spectral changes of $H_2TPP(PE)_8$ upon addition of TBAOH and F^- ion in CH_2Cl_2 at 298 K.	16
Figure S22. (top) $H_2TPP(PE)_4$ in different solvents; (bottom) UV-Visible and spectral shifts of $H_2TPP(PE)_4$ in selected solvents at 298 K.	17
Figure S23. (top) Colorimetric response of $ZnTPP(PE)_8$ in different solvents; (bottom) UV-Visible and fluorescence spectra of $ZnTPP(PE)_8$ in different solvents at 298 K.	17
Table S3. Optical absorption spectral data of $H_2TPP(PE)_4$, $ZnTPP(PE)_4$ and $ZnTPP(PE)_8$ in different solvents at 298 K.	18
Table S4. Fluorescence quantum yield and lifetime data of $H_2TPP(PE)_8$ and $ZnTPP(PE)_8$ in different solvents at 298 K.	19
Figure S24. (a) Stokes shift of $H_2TPP(PE)_8$ in different solvents *vs.* dielectric constant of various solvents ; (b) Emisssion wavelength (cm^{-1}) of $ZnTPP(PE)_8$ *vs.* dielectric constant of different solvent; (c) Lippert-Mataga plot showing Stokes shift as a function of solvent orientation polarisability (Δf) for $H_2TPP(PE)_8$; (d) Lippert-Mataga plot showing emisssion wavelength (cm^{-1}) as a function of solvent orientation polarisability (Δf) for $ZnTPP(PE)_8$.	20
Figure S25. (a) ^1H NMR spectral changes of $H_2TPP(PE)_8$ upon addition of CN^- (green) and F^- ions (blue) in $CDCl_3$ at 298 K; (b) Proposed schematic representation of dianionic species with HA (A = F or CN) and H_2O.	21
Figure S26. (bottom) Differencial Voltamogram (DPV) of $H_2TPP(PE)_8$ in CH_2Cl_2 containing 0.1 M $TBAPF_6$ at 298 K; (top) DPV of $H_2TPP(PE)_8$ in presence of TBAF in CH_2Cl_2 at 298 K. Pt working electrode, Ag/AgCl reference electrode and Pt wire reference electrodes were used.	22
Figure S27. (top) $ZnTPP(PE)_4$ in presence of different anions in CH_2Cl_2 at 298 K; (bottom) UV-Visible of $ZnTPP(PE)_4$ in presence of F^- and CN^- ions in CH_2Cl_2 at 298 K.	23
Table S5. Optical absorption data of spectral data of $H_2TPP(PE)_8$ and $ZnTPP(PE)_4$ in presence of different anions in CH_2Cl_2 at 298 K	23
Figure S28. UV-Visible titration of $ZnTPP(PE)_8$ with (a) Cl^- and (b) OAc^- ions in toluene at 298 K. Inset shows corresponding Hill plots.	24
Figure S29. UV-Visible titration of $ZnTPP(PE)_4$with CN^- ion in toluene at 298 K. Inset shows Hill Plot.	24

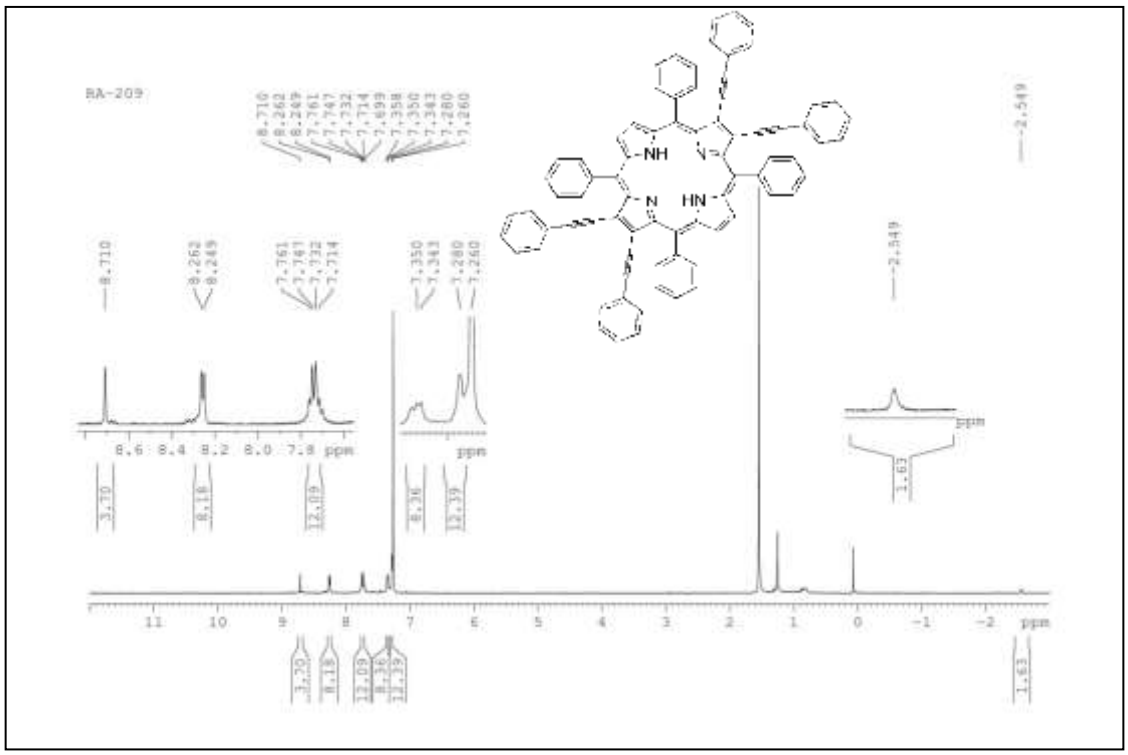

Figure S1. ^{1}H NMR spectrum of $H_2TPP(PE)_4$ in $CDCl_3$ at 298 K

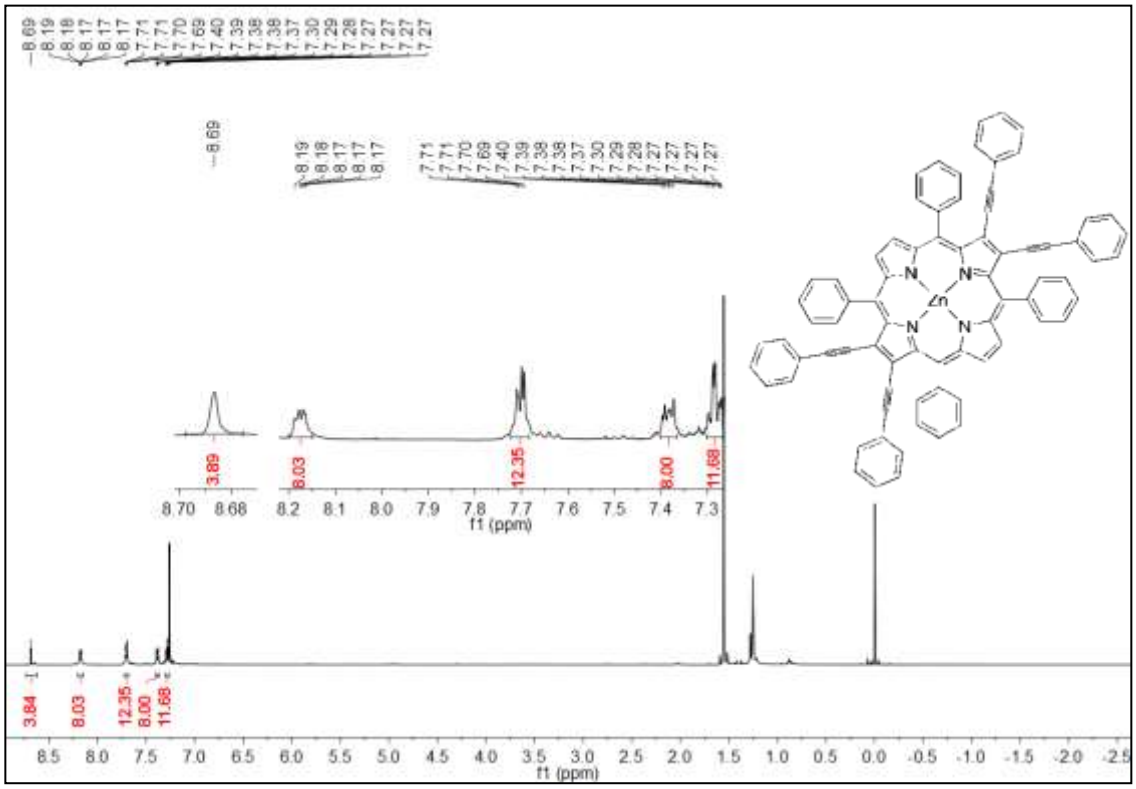

Figure S2. ^{1}H NMR spectrum of $ZnTPP(PE)_4$ in $CDCl_3$ at 298 K.

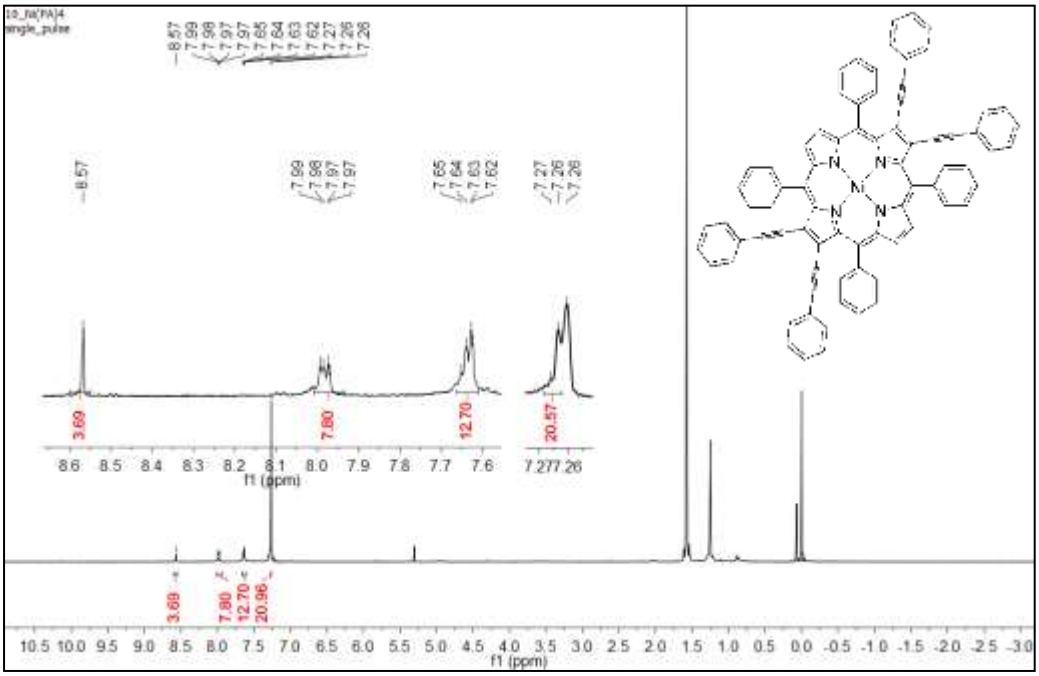

Figure S3. ^{1}H NMR spectrum of NiTPP(PE)$_4$ in $CDCl_3$ at 298 K.

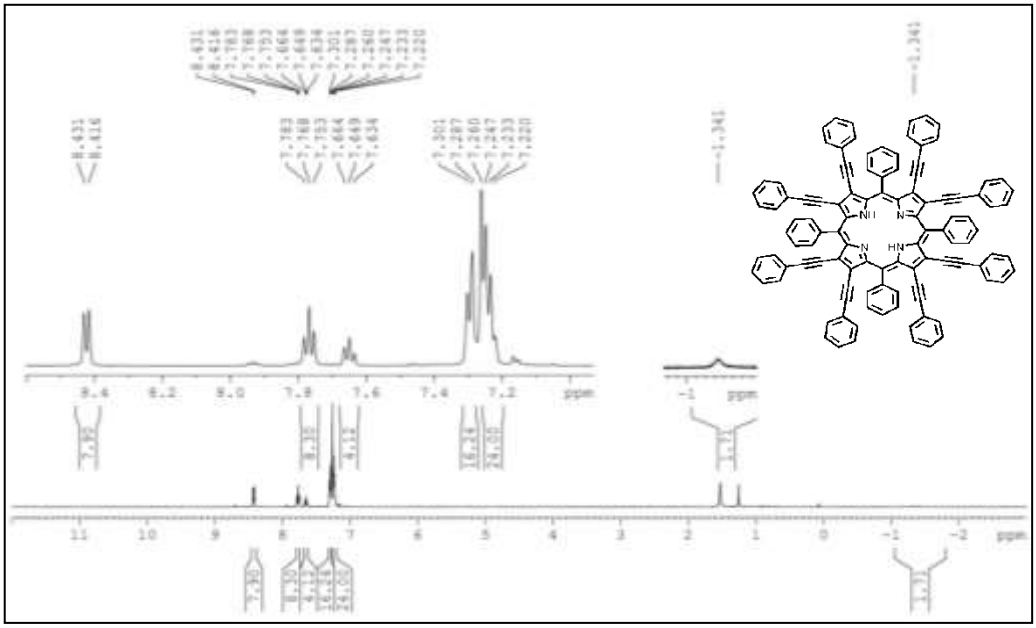

Figure S4. ^{1}H NMR spectrum of H_2TPP(PE)$_8$ in $CDCl_3$ at 298 K.

.

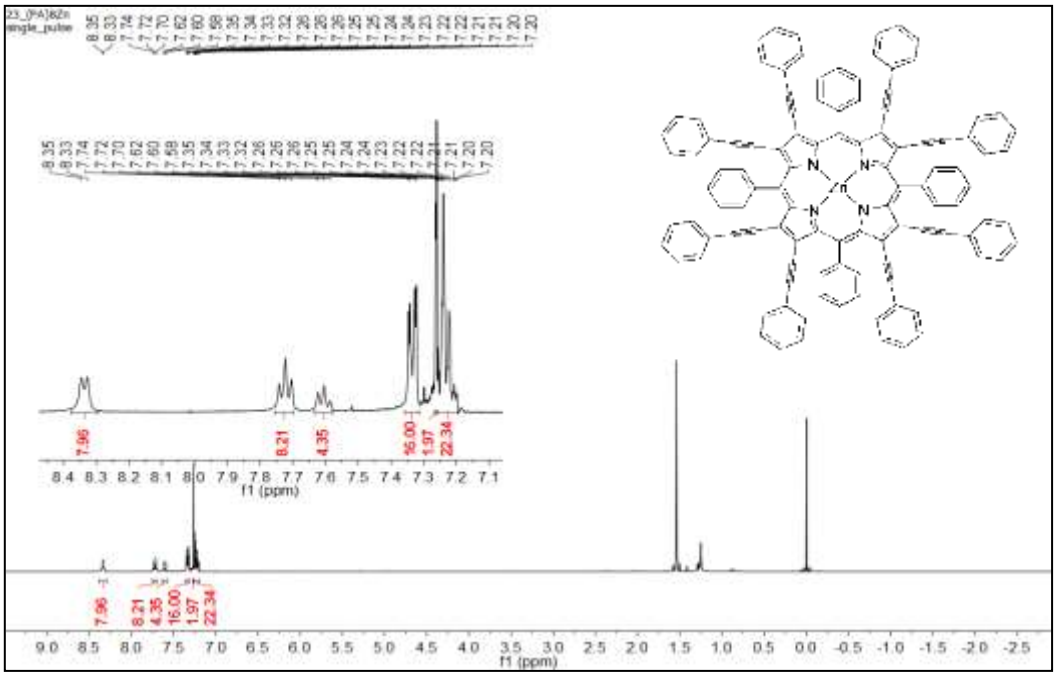

Figure S5. ^{1}H NMR spectrum of ZnTPP(PE)$_8$ in $CDCl_3$ at 298 K

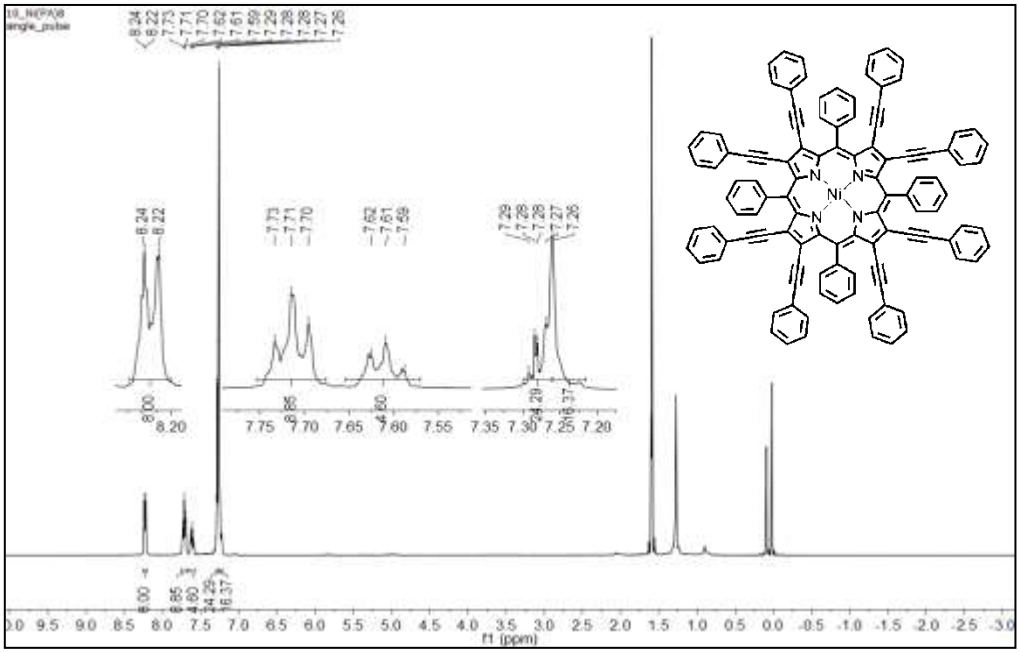

Figure S6. ^{1}H NMR spectrum of NiTPP(PE)$_8$ in $CDCl_3$ at 298 K.

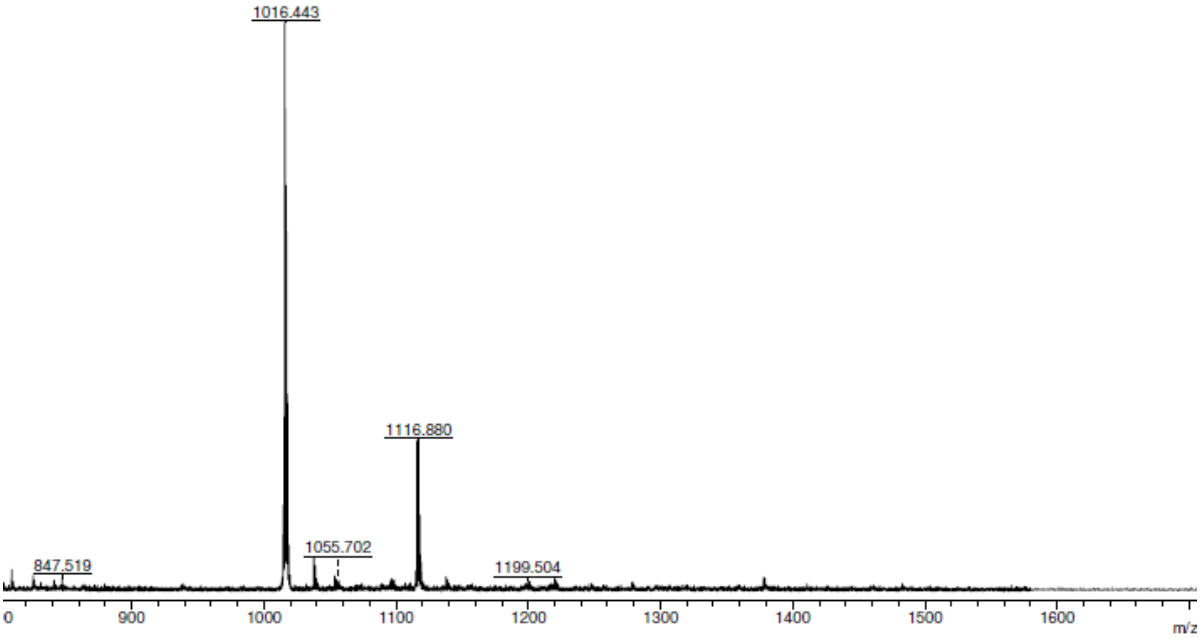

Figure S7. MALDI-TOF mass spectrum of $H_2TPP(PE)_4$

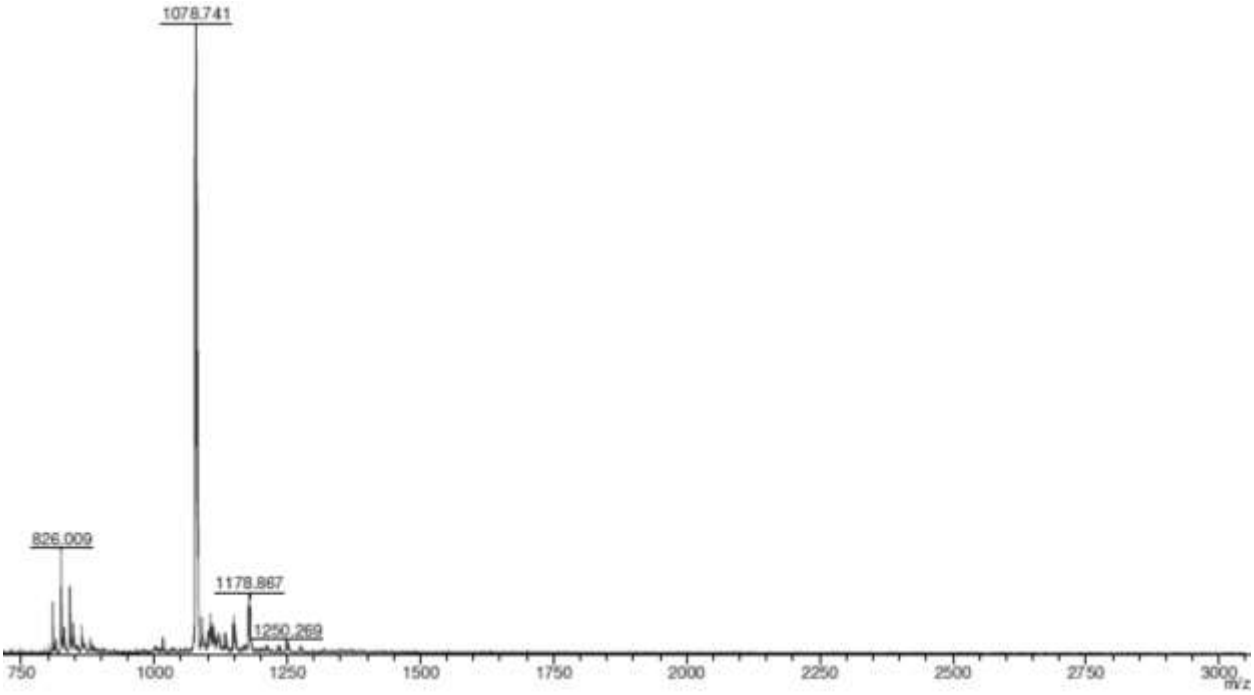

Figure S8. MALDI-TOF mass spectrum of $ZnTPP(PE)_4$

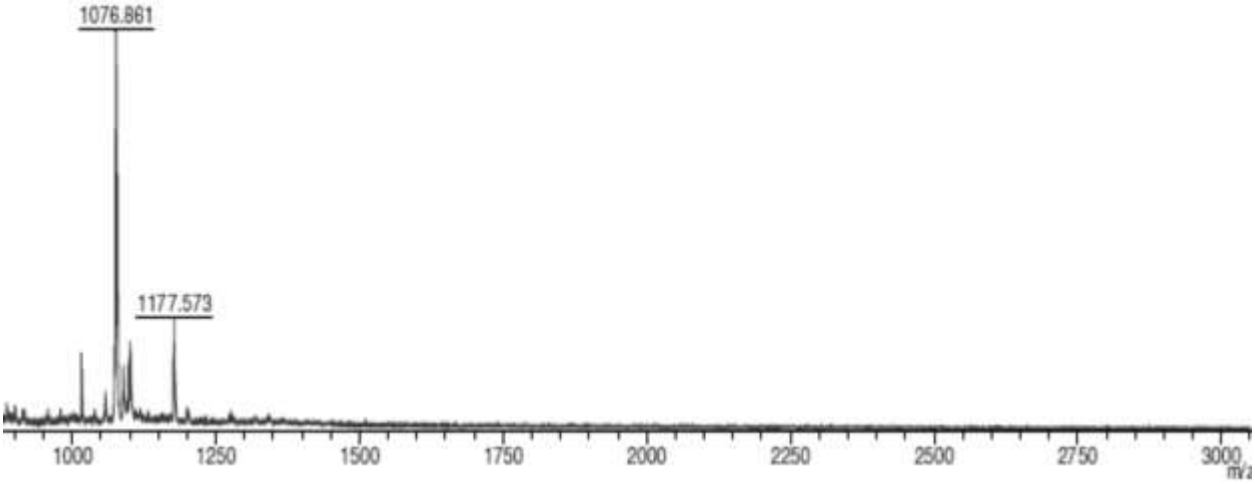

Figure S9. MALDI-TOF mass spectrum of CuTPP(PE)$_4$

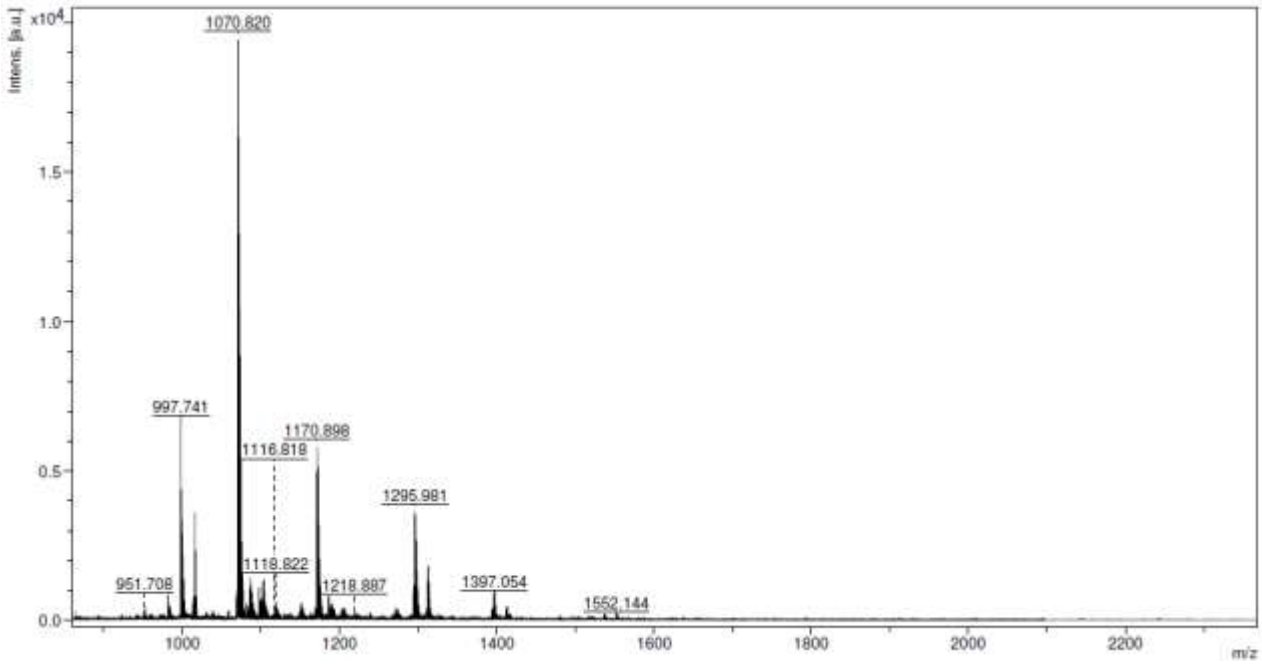

Figure S10. MALDI-TOF mass spectrum of NiTPP(PE)$_4$

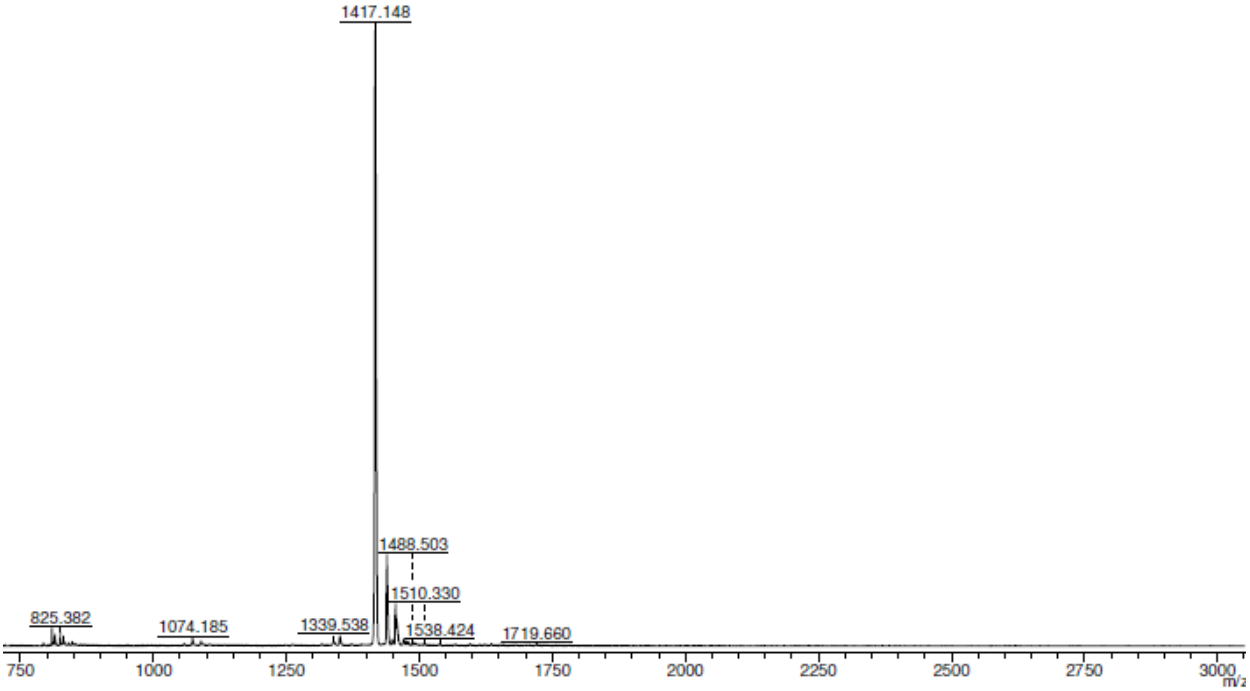

Figure S11. MALDI-TOF mass spectrum of $H_2TPP(PE)_8$

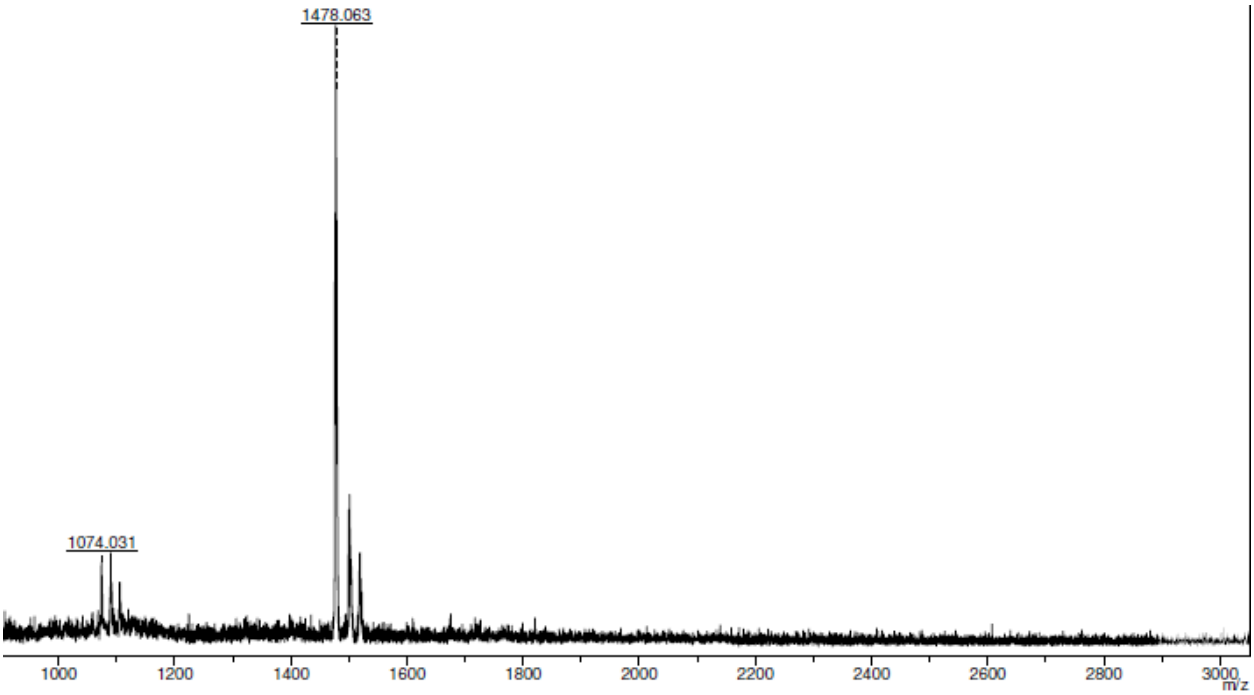

Figure S12. MALDI-TOF mass spectrum of $CuTPP(PE)_8$

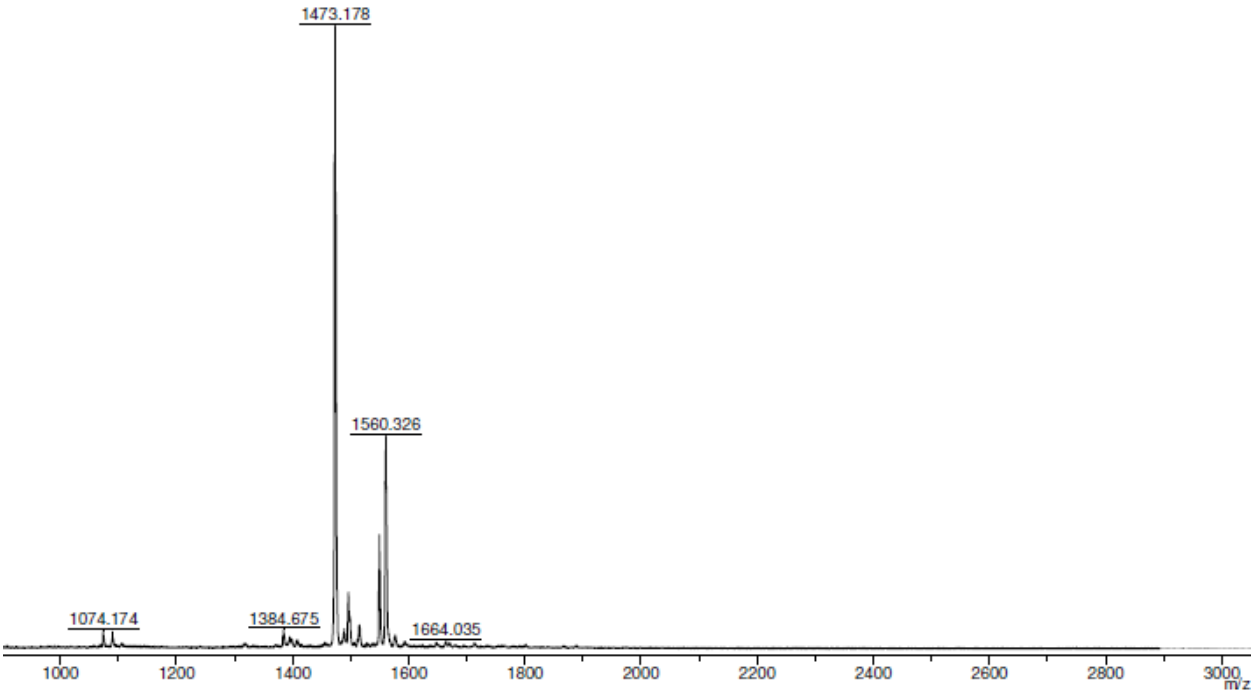

Figure S13. MALDI-TOF mass spectrum of $CoTPP(PE)_8$

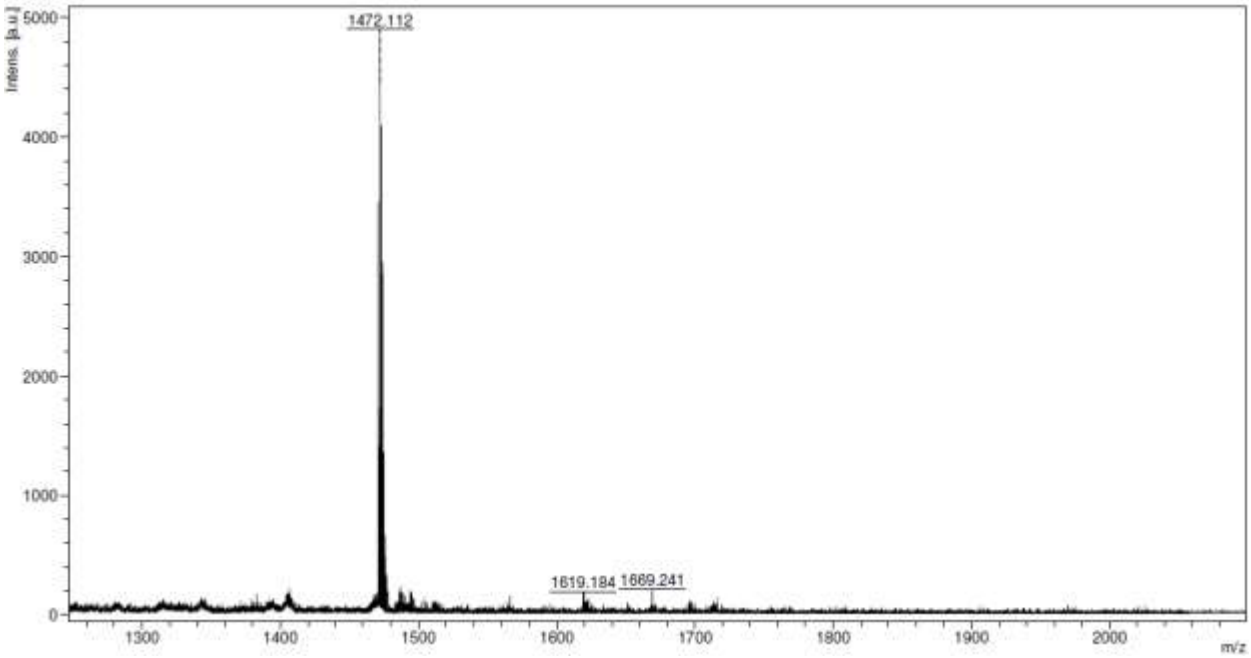

Figure S14. MALDI-TOF mass spectrum of $NiTPP(PE)_8$

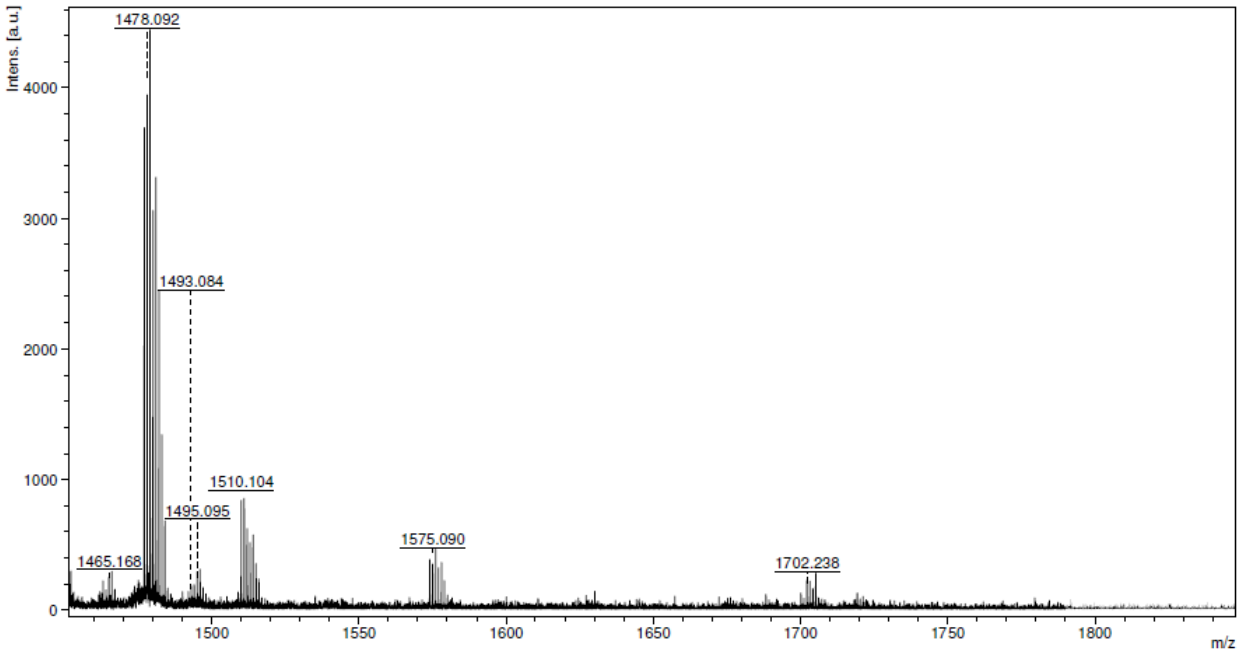

Figure S15. MALDI-TOF mass spectrum of ZnTPP(PE)$_{8.}$

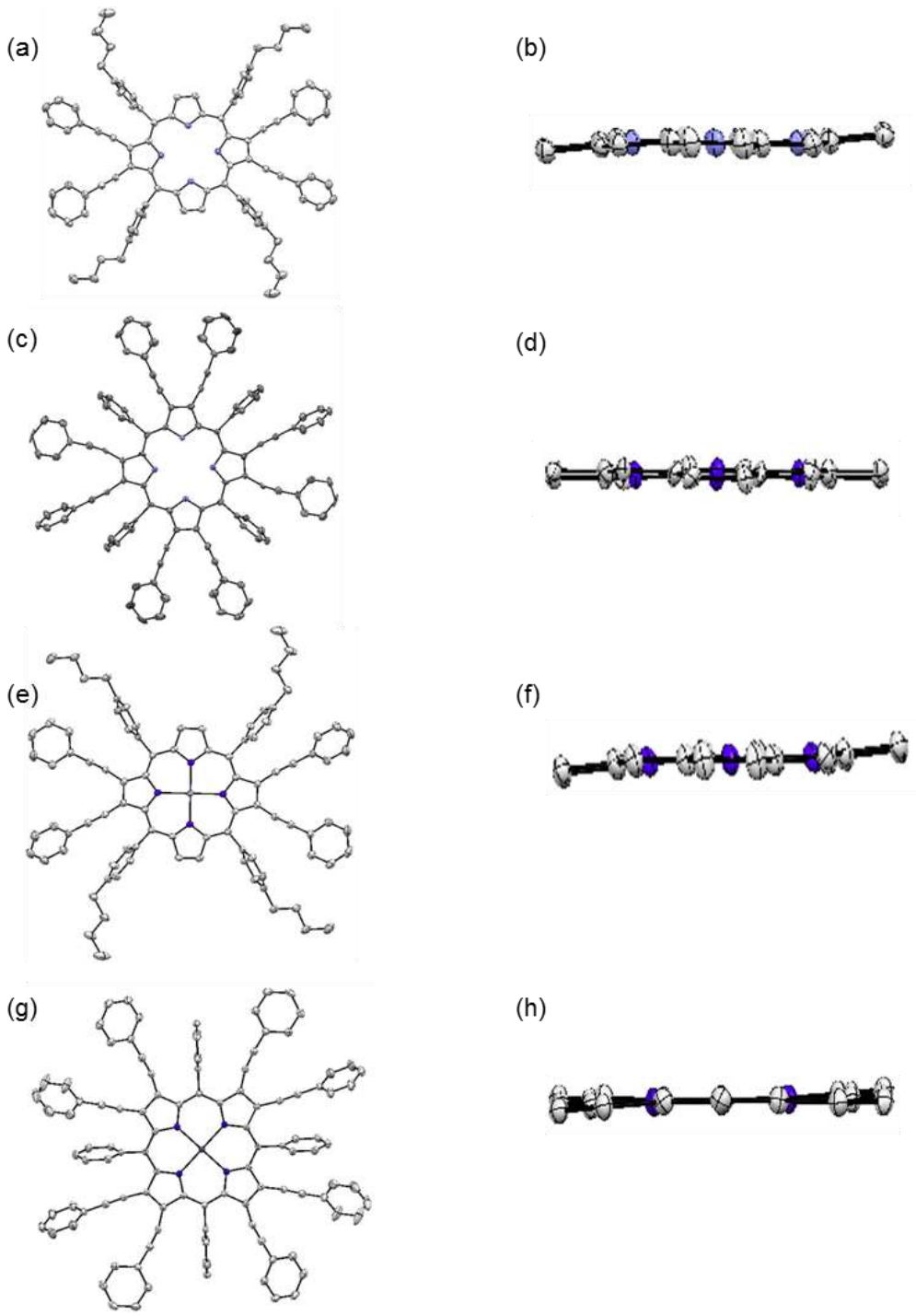

Figure S16. The ORTEP diagrams showing top and side views of $H_2T(4\text{-BuPh})P(PE)_4$ (a and b); $H_2TPP(PE)_8$ (c and d) ; $ZnTPP(PE)_4$ (e and f) and $ZnTPP(PE)_8$(g and h). The solvates are not shown for clarity, and in side view, the *β*-substituents and *meso*-phenyl groups are not shown for clarity.Crystal structures data for $H_2T(4\text{-BuPh})P(PE)_4$ is taken from P. Bhyrappa *et al.*,*Eur. J. Inorg. Chem.*, 2014, 5760-5770 and for $MTPP(PE)_8$ T. Chandra *et al*., *Inorg. Chem.* 2003, **42**, 5158-5172.

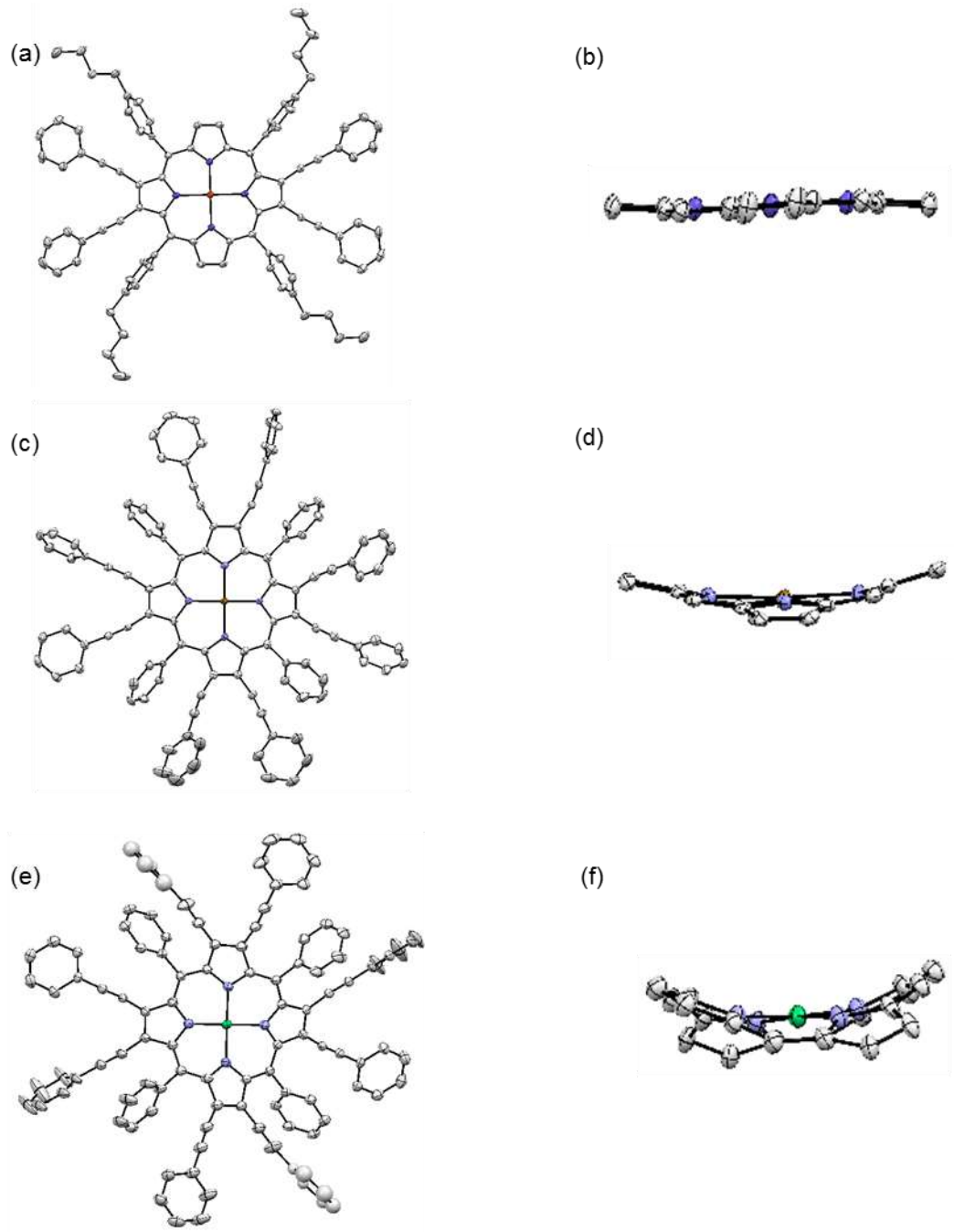

Figure S17. The ORTEP diagrams showing top and side views of CuT(4-BuPh)P(PE)$_4$ (a and b); CuTPP(PE)$_8$ (c and d) and NiTPP(PE)$_8$ (e and f). The solvates are not shown for clarity, and in side view, the β-substituents and *meso*-phenyl groups are not shown for clarity.Crystal structures data for H_2T(4-BuPh)P(PE)$_4$ is taken from P. Bhyrappa *et al.*,*Eur. J. Inorg. Chem.*, 2014, 5760-5770 and for MTPP(PE)$_8$ T. Chandra *et al*., *Inorg. Chem.* 2003, **42**, 5158-5172.

Table S1. Crystal structure data of*β*-phenylethynyl substituted porphyrins from literature.[a,b]

Porphyrin	**ΔC_β**	**Δ24**	**ΔMetal**	**Remarks**
$H_2T(4\text{-BuPh})P(PE)_4$[a]	0.058	0.086	-	Planar
$H_2TPP(PE)_8$[b]	0.094	0.068	-	Planar
$ZnT(4\text{-BuPh})P(PE)_4$[a]	0.051	0.042	0.00	Planar
$ZnTPP(PE)_8$[b]	0.040	0.032	0.00	Planar
$CuT(4\text{-BuPh})P(PE)_4$[a]	0.056	0.046	0.00	Planar
$CuTPP(PE)_8$[b]	0.578	0.287	0.008	Nonplanar
$NiTPP(PE)_8$[b]	0.700	0.470	0.011	Nonplanar

[a]Crystal structures data is taken from P. Bhyrappa, U. K. Sarangi, V. Velkannan and V. Ramkumar, *Eur. J. Inorg. Chem.*, 2014, 5760-5770; [b]Crystal structures data is taken fromT. Chandra, B. J. Kraft, J. C. Huffman, J. M. Zaleski, *Inorg. Chem.* 2003, **42**, 5158-5172.

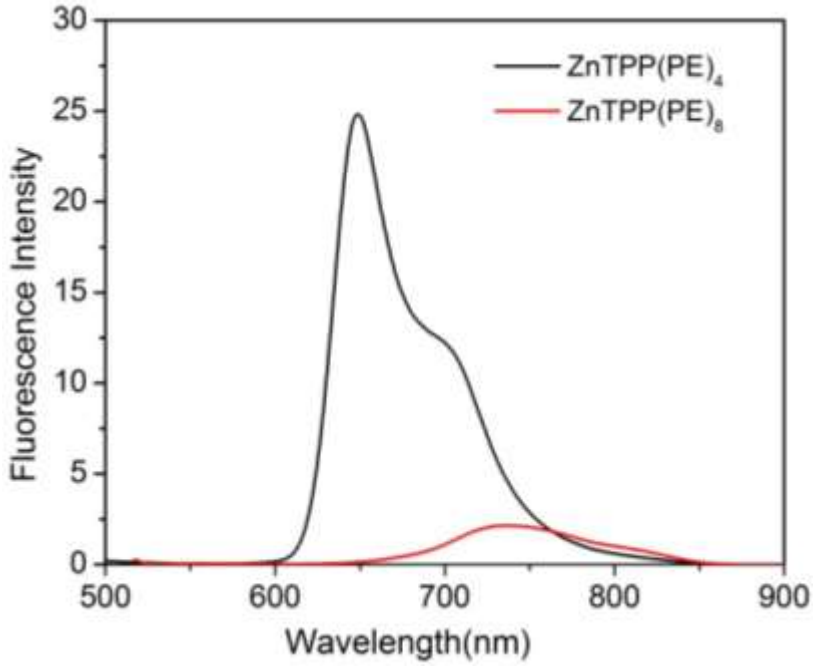

Figure S18. Fluorescence spectra of $ZnTPP(PE)_n$ (n = 4 and 8) in CH_2Cl_2 at 298 K.

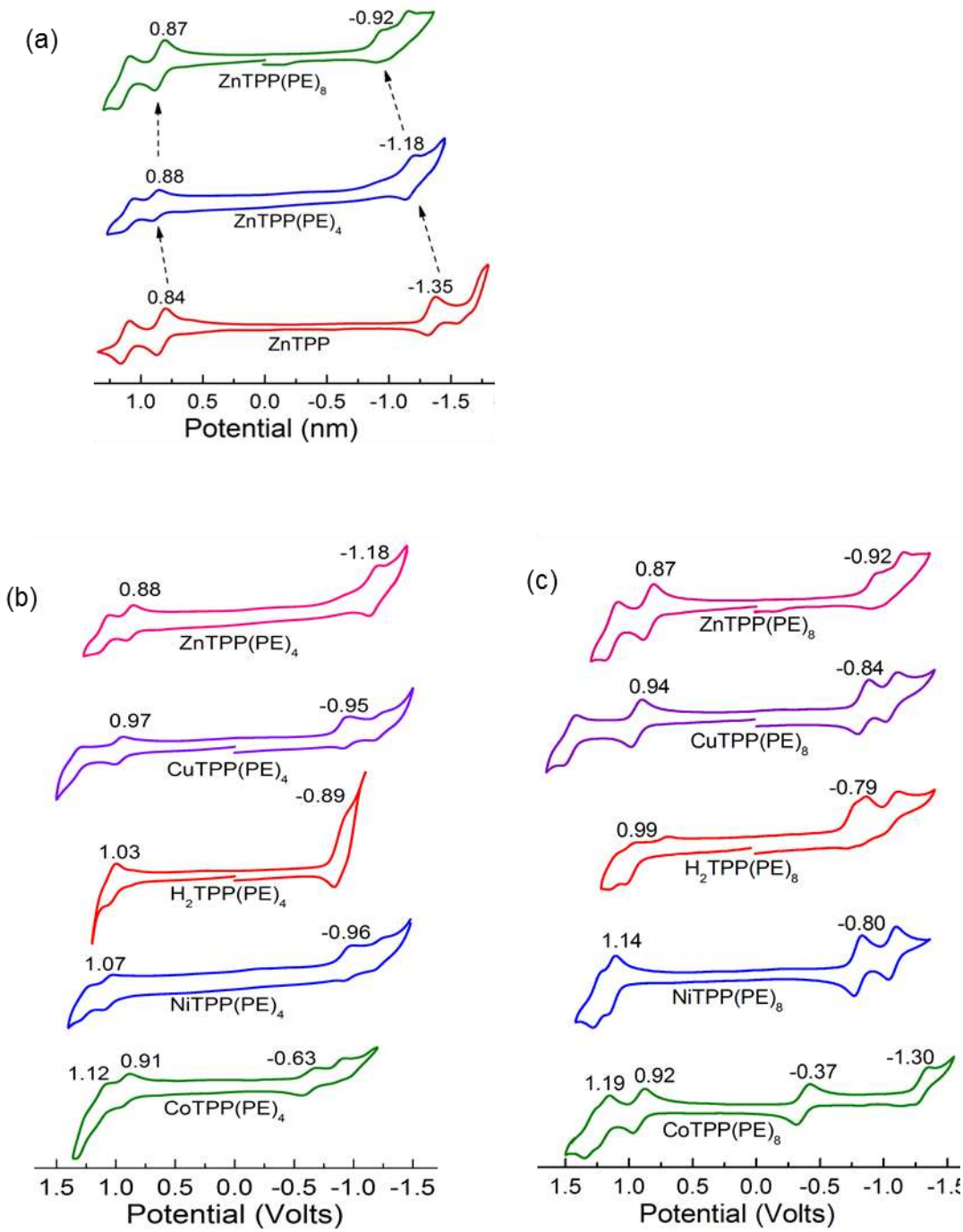

Figure S19. Cyclic Voltammograms of (a) $ZnTPP(PE)_n$ (n = 0, 4 and 8); (b) $MTPP(PE)_4$; (c) $MTPP(PE)_8$ where M = 2H, Co(II), Ni(II), Cu(II) and Zn(II); in CH_2Cl_2 containing 0.1 M $TBAPF_6$ using Ag/AgCl as reference electrode with a scan rate of 0.1 V/sat 298 K.

Table S2. Electrochemical redox data (*vs*Ag/AgCl)of $CoTPP(PE)_n$ (n = 0, 4 and 8) using 0.1 M $TBAPF_6$with a scan rate of 0.1 V/s at 298 K.

Porphyrin	Oxidation		Reduction		Metal Centered	
	I	II	I	II	$Co^{II/III}$	$Co^{II/I}$
CoTPP	1.06	1.32	-1.38	-	0.85	-0.86
$CoTPP(PE)_4$	1.12	-	-	-	0.91	-0.63
$CoTPP(PE)_8$	1.19	1.31	-1.30	-	0.92	-0.37

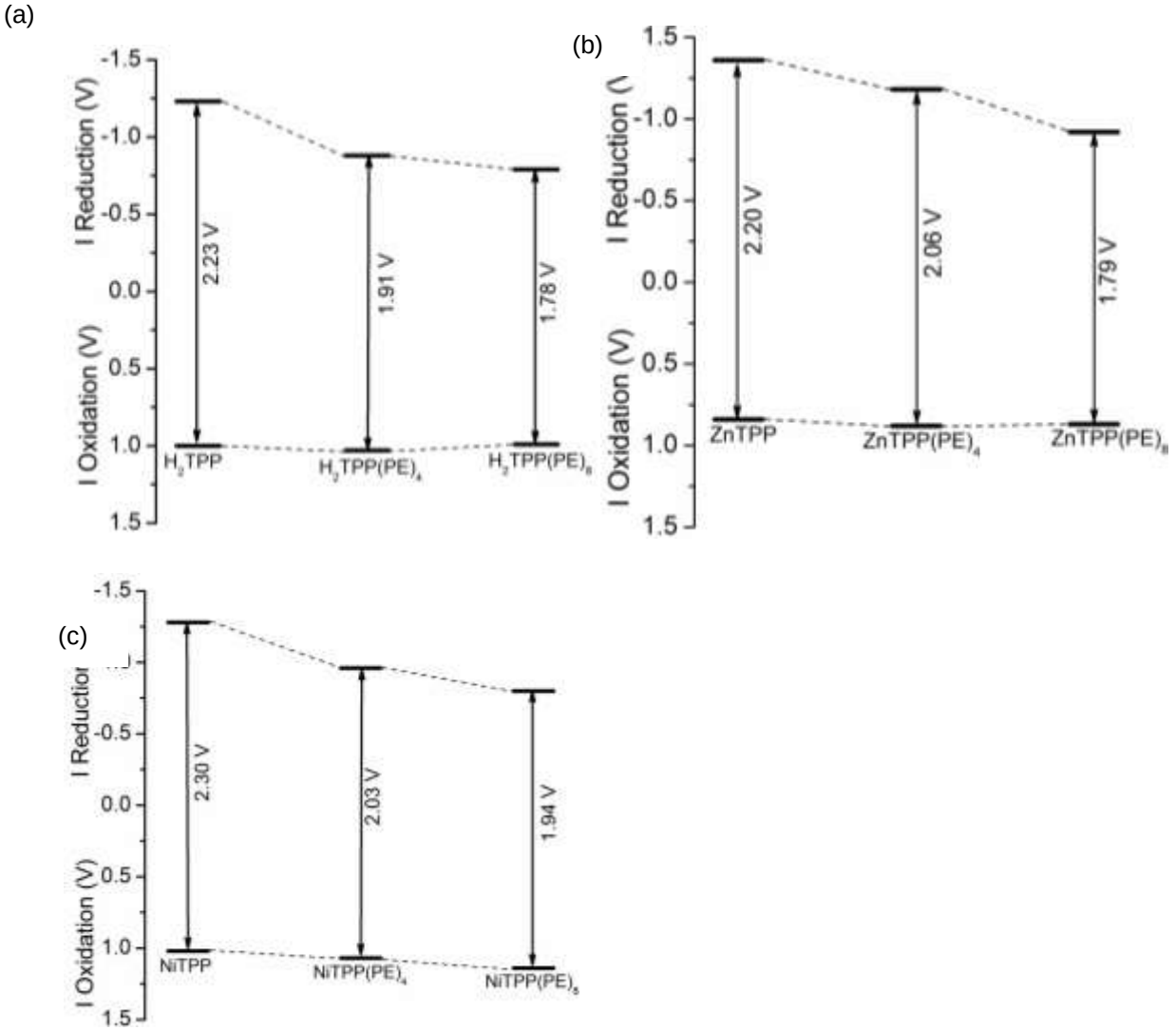

Figure S20. HOMO-LUMO gap variation in $MTPP(PE)_n$ (M = 2H, Zn(II) and Ni(II); n = 0, 4 and 8).

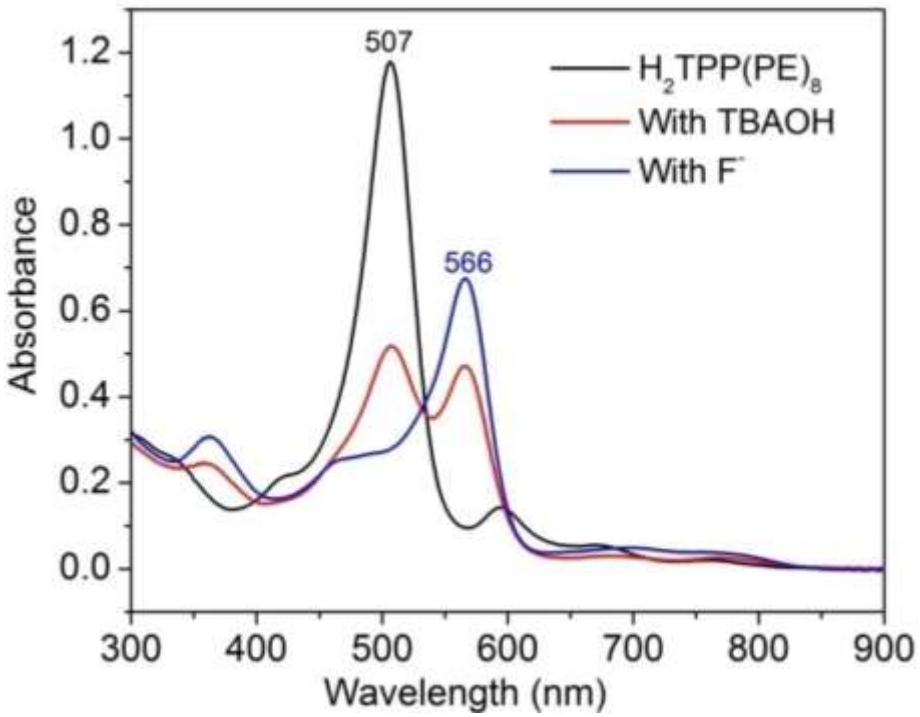

Figure S21. UV-Visible spectral changes of $H_2TPP(PE)_8$ upon addition of TBAOH and F^- ion in CH_2Cl_2 at 298 K.

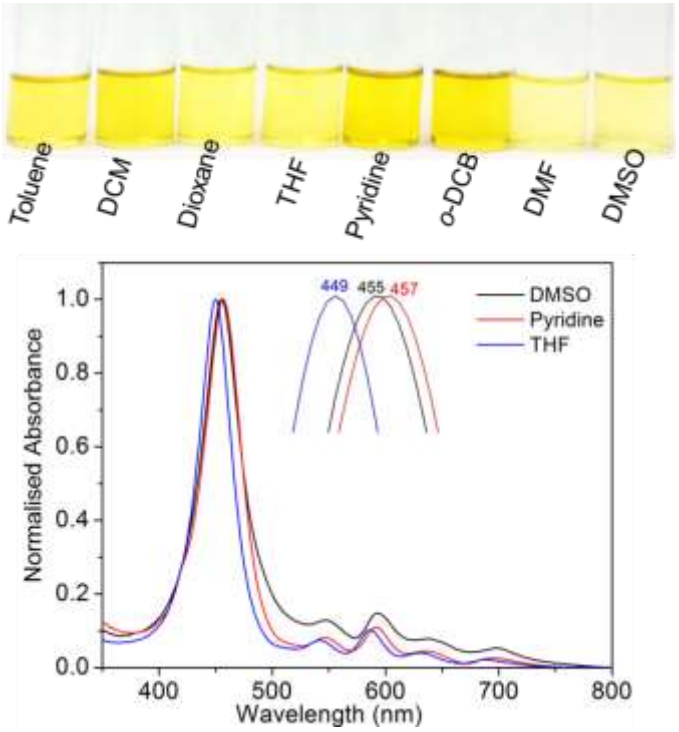

Figure S22. (top) $H_2TPP(PE)_4$ in different solvents; (bottom) UV-Visible and spectralshifts of $H_2TPP(PE)_4$ in selected solvents at 298 K.

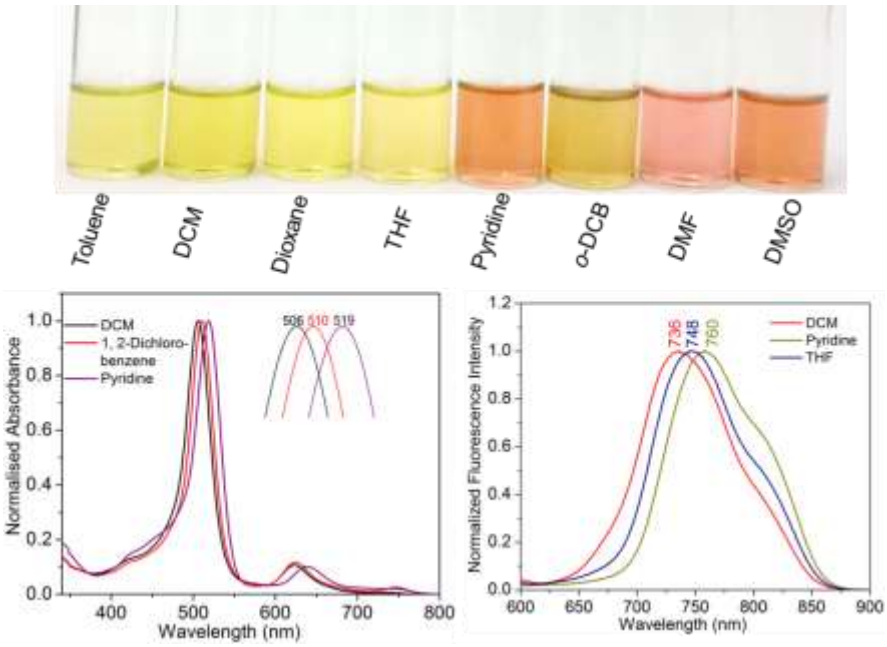

Figure S23. (top) Colorimetric response of $ZnTPP(PE)_8$ in different solvents; (bottom) UV-Visible and fluorescence spectra of $ZnTPP(PE)_8$ in different solvents at 298 K.

Table S3. Optical absorption spectral data of $H_2TPP(PE)_4$, $ZnTPP(PE)_4$ and $ZnTPP(PE)_8$ in different solvents at 298 K.

$H_2TPP(PE)_4$			
Solvent	B band, nm	Q band(s), nm	Emission, nm
Toluene	454(5.05)	544(3.93), 588(4.09), 633(3.67), 691(3.40)	729
DCM	453(5.57)	545(4.44),590(4.58), 633(4.20), 691(3.96)	739
1,4-Dioxane	452(5.07)	544(3.95), 588(4.09), 633(3.70), 690(3.47)	747
THF	450(4.92)	543(3.79), 587(3.93), 631(3.53), 689(3.26)	734
Pyridine	457(4.99)	547(3.90), 592(4.04), 637(3.64), 693(3.40)	745
o-Dichlorobenzene	458(5.02)	546(3.96), 592(4.12), 637(3.73), 694(3.48)	732
DMF	453(4.99)	545(3.98), 589(4.09), 632(3.81), 688(3.68)	793
DMSO	455(4.83)	548(3.93), 593(3.99), 639(3.72), 699(3.55)	703, 787
$ZnTPP(PE)_4$			
Toluene	463(5.37)	583(4.16), 631(4.63)	643
DCM	458(5.48)	581(4.26), 630(4.68)	644
1,4-Dioxane	466(5.41)	589(4.20), 635(4.61)	651
THF	465(5.47)	589(4.25), 636(4.67)	652, 709
Pyridine	476(5.36)	598(4.15), 645(4.56)	671, 716
o-Dichlorobenzene	464(5.30)	584(4.03), 633(4.56)	645
DMF	470(5.54)	593(4.33), 641(4.73)	663, 715
DMSO	473(5.52)	595(4.27), 642(4.71)	664, 715
$ZnTPP(PE)_8$			
Toluene	508(5.53)	624(4.58)	736
DCM	506(5.52)	623(4.54)	736
1,4-Dioxane	506(5.41)	625(4.44), 739(3.84)	743
THF	508(5.44)	628)(4.45), 740(3.77)	748
Pyridine	519(5.35)	639(4.34), 745(3.66)	759
o-Dichlorobenzene	510(5.34)	624(4.41), 747(3.73)	740
DMF	519(5.39)	641(4.37)	762
DMSO	517(5.39)	637(4.39)	761

Values in parentheses refers to logε (ε in Mol^{-1} cm^{-1}).

Table S4. Fluorescence quantum yield and lifetime data of $H_2TPP(PE)_8$ and $ZnTPP(PE)_8$ in different solvents at 298 K.

Porphyrin	Solvent	$\lambda_{em, nm}$	Stokes shift (cm^{-1})	Φ_f	τ (ns)	χ^2
$H_2TPP(PE)_8$	Toluene	810	829.55	3.6×10^{-3}	1.63	1.12
	DCM	814	838.35	5.2×10^{-3}	1.44	0.84
	1,4-Dioxane	820	911.04	2.7×10^{-3}	1.47	1.09
	THF	823	1007.23	1.9×10^{-3}	1.45	1.12
	Pyridine	826	965.36	2.4×10^{-3}	0.23(27.54%) 1.31(67.46%) 5.58(5.0%)	1.01
	o-DCB	809	796.95	3.5×10^{-3}	1.59	1.07
	DMF	765	1677.37	1.6×10^{-3}	0.66(73.15%) 2.26(26.85%)	1.12
	DMSO	839	2552.83	0.43×10^{-3}	1.13(64.49%) 2.96(5.97%) 0.17(29.54%)	1.09
$ZnTPP(PE)_8$	Toluene	736	2,438.68	2.2×10^{-3}	1.24	1.18
	DCM	736	2,464.41	2.4×10^{-3}	0.97	1.01
	1,4-Dioxane	743	72.84	3.1×10^{-3}	1.40	1.31
	THF	748	144.53	2.8×10^{-3}	1.01	1.19
	Pyridine	759	247.59	4.3×10^{-3}	0.77(39.70%) 1.57(60.30%)	0.99
	o-DCB	740	-126.63	2.3×10^{-3}	1.39	1.27
	DMF	762	2,477.26	3.7×10^{-3}	0.75(43.55%) 1.73(56.45%)	0.96
	DMSO	761	2,557.98	3.6×10^{-3}	0.39(24.44%) 1.45(75.56%)	0.98

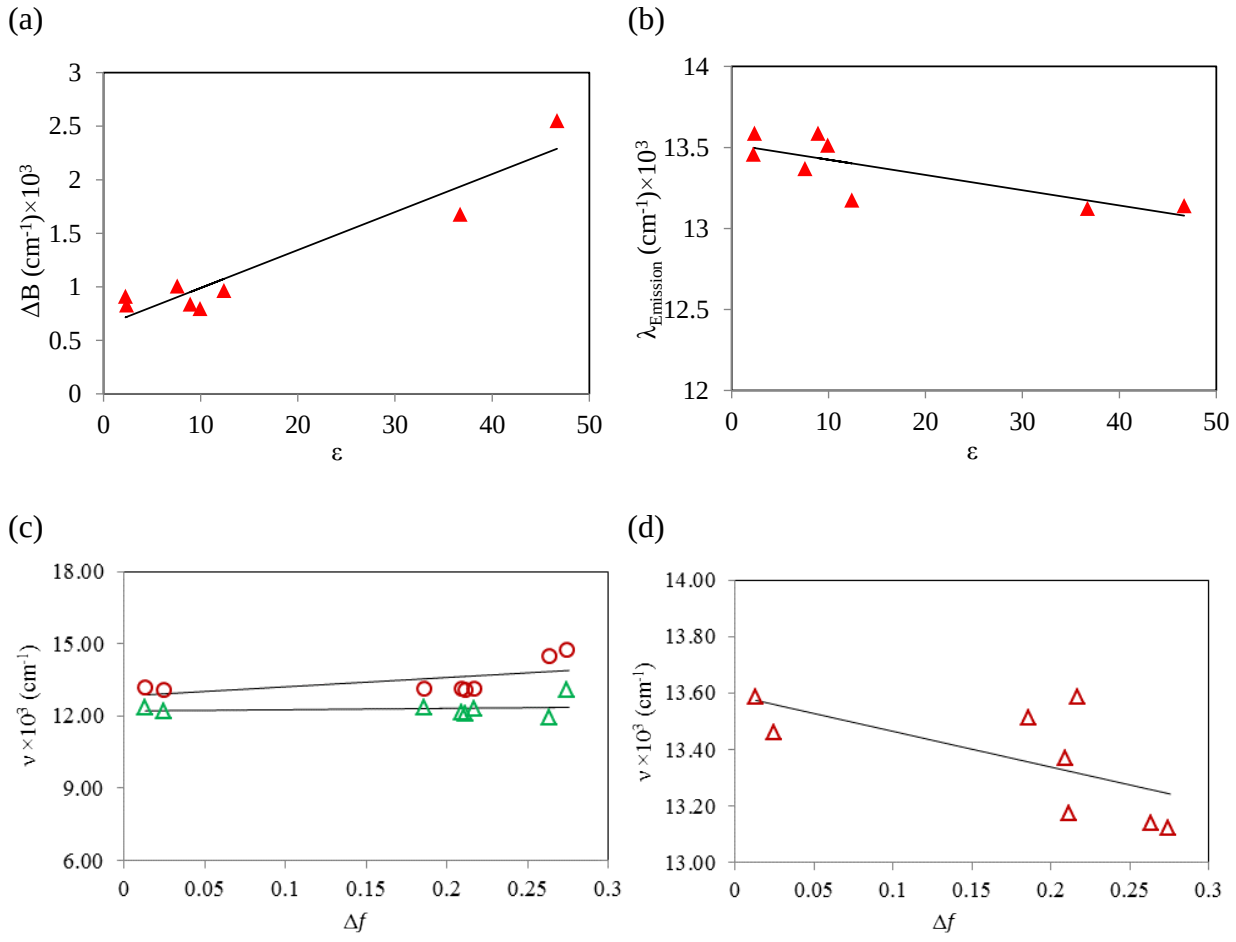

Figure S24. (a) Stokes shift of $H_2TPP(PE)_8$ in different solvents *vs.* dielectric constant of various solvents ; (b) Emisssion wavelength (cm^{-1}) of $ZnTPP(PE)_8$ *vs.* dielectric constant of different solvent; (c) Lippert-Mataga plot showing Stokes shift as a function of solvent orientation polarisability (Δf) for $H_2TPP(PE)_8$; (d) Lippert-Mataga plot showing emisssion wavelength (cm^{-1}) as a function of solvent orientation polarisability (Δf) for $ZnTPP(PE)_8$.

(a)

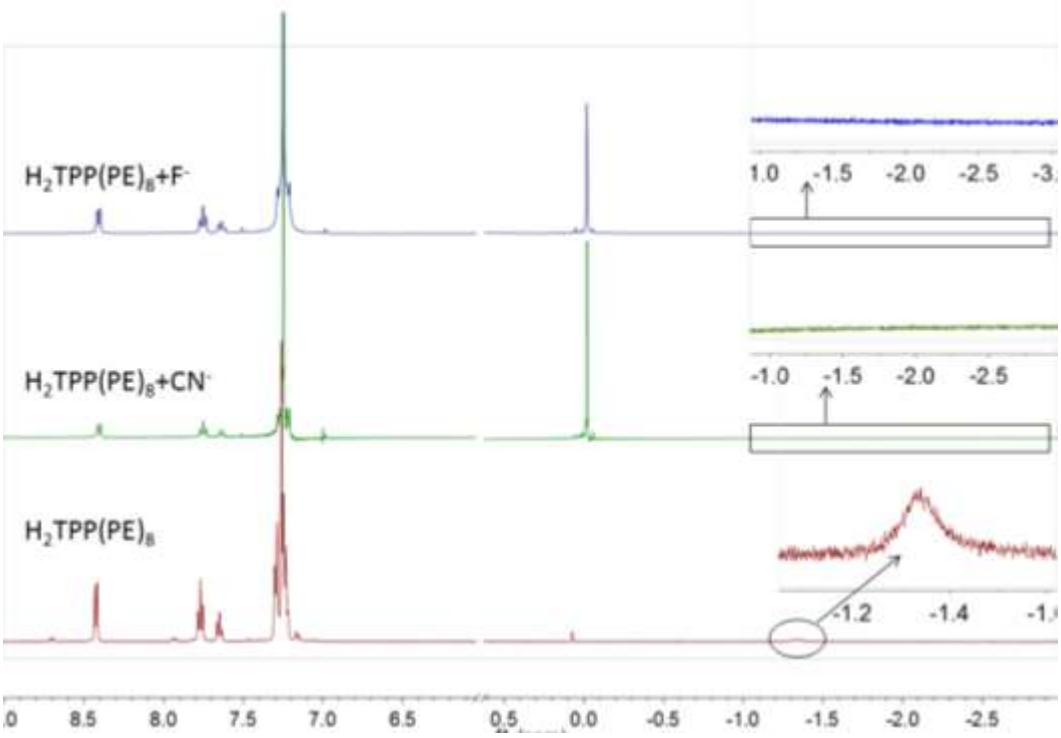

(b)

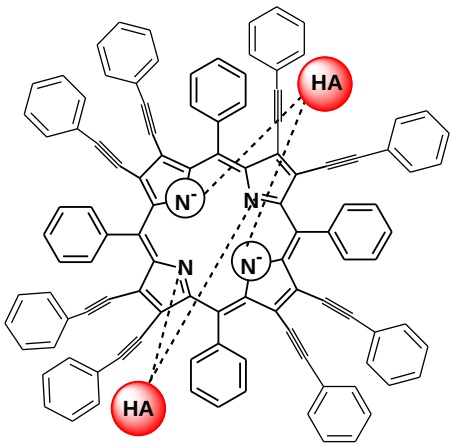

A = F or CN

$$H_2TPP(PE)_8 + OH^- \rightleftharpoons [TPP(PE)_8]^{2-} + H_2O$$

Figure S25. (a) ^{1}H NMR spectral changes of $H_2TPP(PE)_8$ upon addition of CN^- (green) and F^- ions (blue) in $CDCl_3$ at 298 K; (b) Proposed schematic representation of dianionic species with HA (A = F or CN) and H_2O.

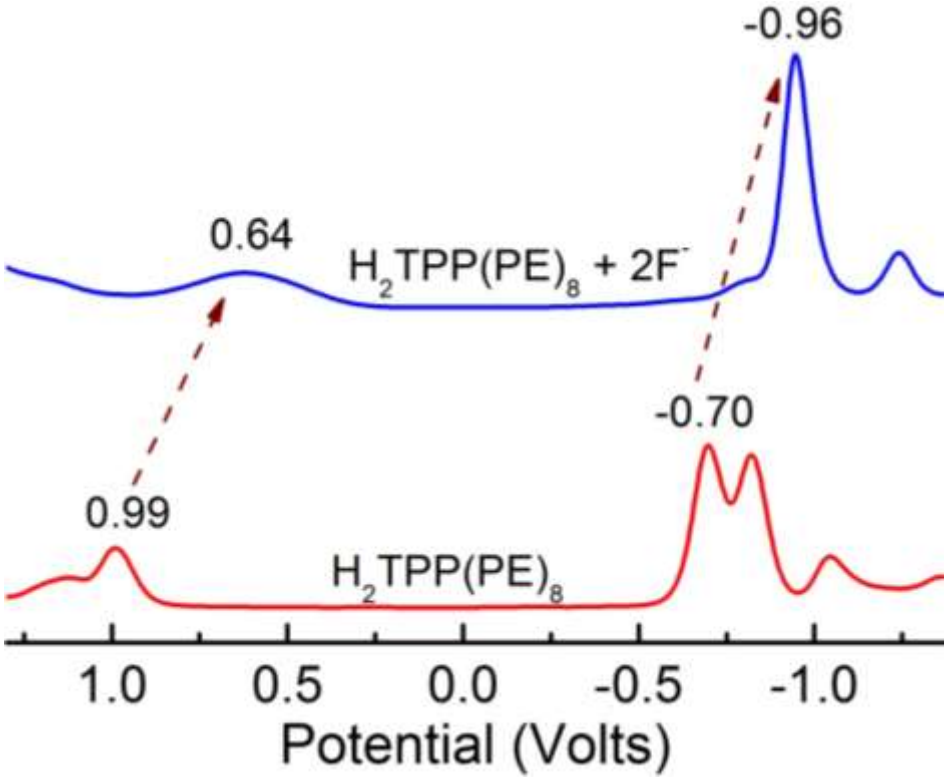

Figure S26. (bottom) Differencial Voltamogram (DPV) of $H_2TPP(PE)_8$ in CH_2Cl_2 containing 0.1 M $TBAPF_6$ at 298 K; (top) DPV of $H_2TPP(PE)_8$ in presence of TBAF in CH_2Cl_2 at 298 K. Pt working electrode, Ag/AgCl reference electrode and Pt wire reference electrodes were used.

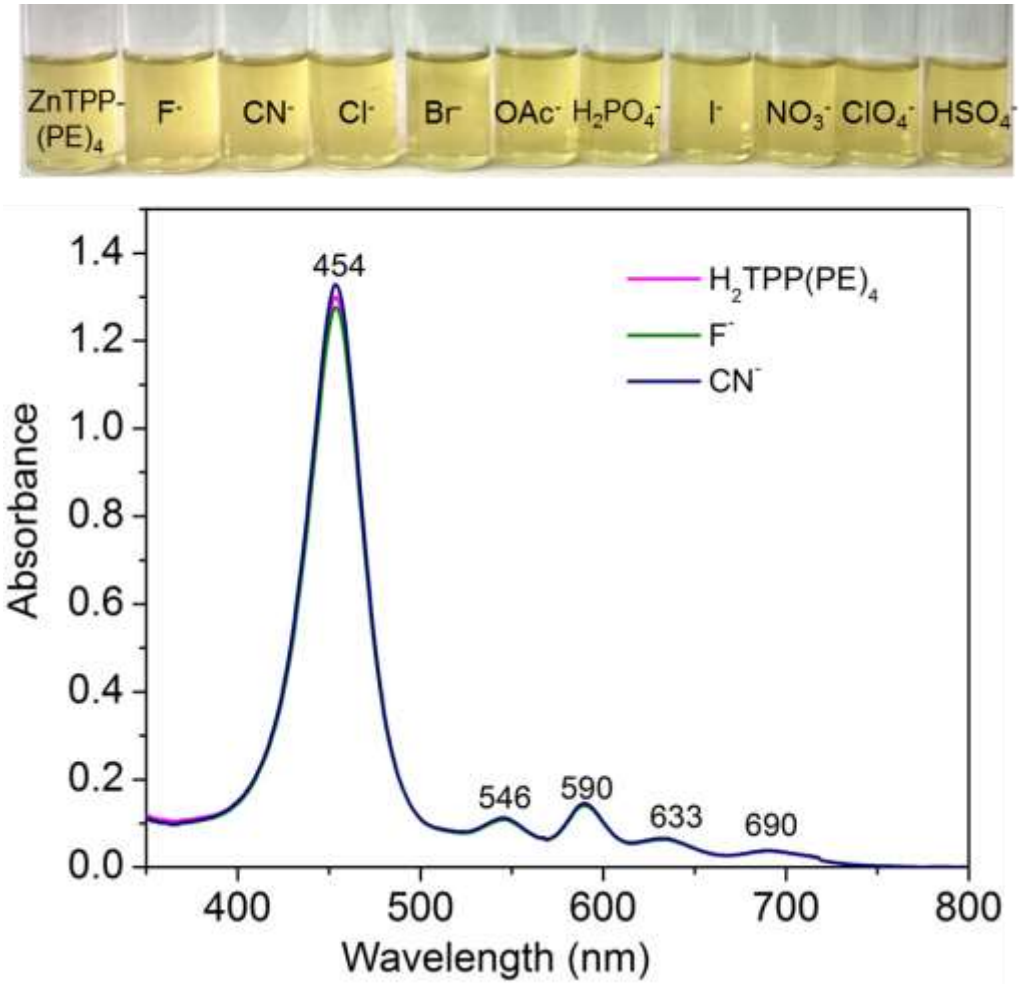

Figure S27. (top) ZnTPP(PE)$_4$ in presence of different anions in CH_2Cl_2 at 298 K; (bottom) UV-Visible of ZnTPP(PE)$_4$ in presence of F^- and CN^- ions in CH_2Cl_2 at 298 K.

Table S5. Optical absorption data of spectral data of H_2TPP(PE)$_8$ and ZnTPP(PE)$_4$ in presence of different anions in CH_2Cl_2at 298 K.

H_2TPP(PE)$_8$	507(5.41)	595(4.48), 672(3.96), 762(3.44)
F^-	566(5.29	688(4.15), 772(3.98)
CN^-	566(5.04)	684(4.01), 770(3.87)
ZnTPP(PE)$_4$	458(5.48)	581(4.26), 630(4.68)
F^-	480(5.47)	602(4.15), 652(4.62)
CN^-	487(5.44)	660(4.46)
CH_3COO^-	464(5.24), 479(5.33)	651(4.46)
$H_2PO_4^-$	462(5.33)	633(4.43)
Cl^-	483(5.39)	654(4.49)

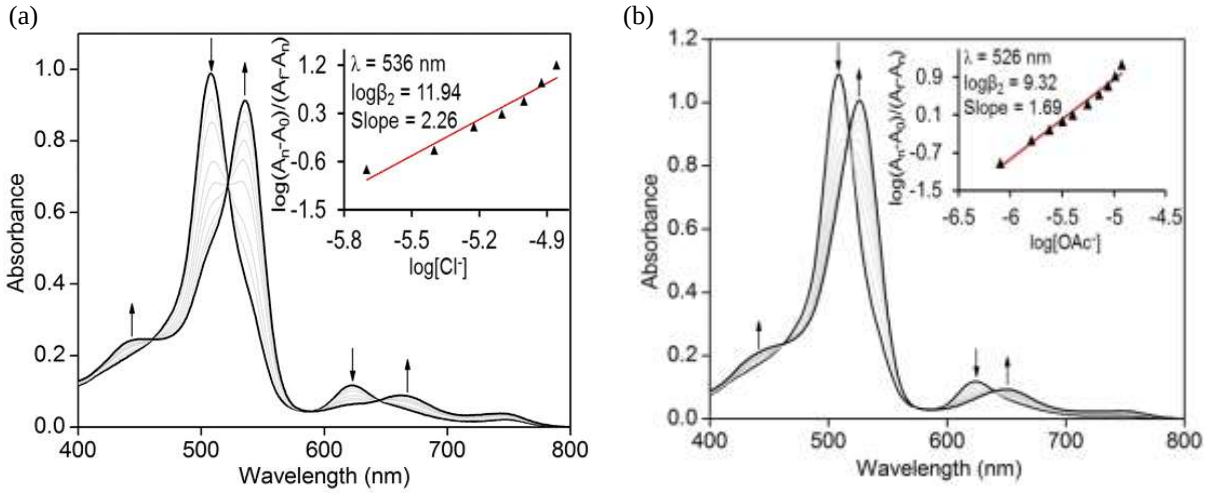

Figure S28.UV-Visible titration of $ZnTPP(PE)_8$ with (a) Cl^- and (b) OAc^- ions in toluene at 298 K. Inset shows corresponding Hill plots.

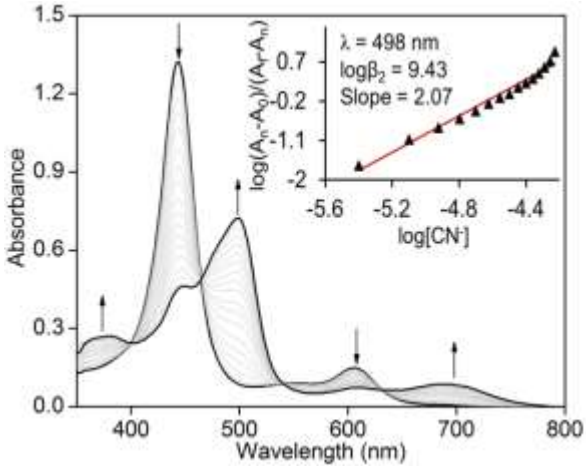

Figure S29.UV-Visible titration of $ZnTPP(PE)_4$with CN^- ion in toluene at 298 K. Inset shows Hill Plot.